Defence Science Journal, Vol. 73, No. 5, September 2023, pp. 612-624, DOI : 10.14429/dsj.73.5.18617
© 2023, DESIDOC

Effect of Twin Island Configuration on Airwake Aerodynamics over Generic Aircraft Carrier Using CFD

Ankit Nehra* and Vijayakumar Rajagopalan

#*Department of Ocean Engineering, IIT Madras, Chennai - 600 036, India*
**E-mail: ankitnehra2008@gmail.com*

ABSTRACT

The technological advancements have led to the evolution of numerous concepts in an aircraft carrier's top-deck design, the twin island concept being the latest entrant. An aircraft carrier's bluff body geometry presents many challenges to the pilot, landing on deck being the most critical. The present study aims to undertake a computational investigation of the aerodynamic analysis of a Twin Island GAC (Generic Aircraft Carrier) conceptualized vis-à-vis its base variant. The flow over the twin island GAC flight deck and downstream is analysed using various transverse planes perpendicular to the flow direction as detailed in the paper. Subsequently, a parametric study was undertaken for understanding the effects of longitudinal translations of the two islands with respect to the baseline GAC position. The results depict the advantage of certain variants of twin islands over a single island, and ~68 % reduction in turbulence is achieved along the glideslope by one of the variations which could aid in reducing pilot workload. The data can act as a catalyst for utilization and incorporation in future floating platform designs and further studies in this field.

Keywords: Twin Island; GAC; CFD; Pilot workload; Aircraft carrier landing

NOMENCLATURE

U	: Free-stream velocity (m/s)
u, v, w	: Velocity components in X, Y, Z direction
V_{ship}	: Ship velocity (m/s)
ρ	: Density of air
L_s	: Length of ship
y^+	: Non-dimensional wall distance
k	: Turbulent kinetic energy ($m^2 s^{-2}$)
ω	: Specific turbulent dissipation rate (s^{-1})
X, Y, Z	: Longitudinal, Transverse, and Vertical co-ordinates
u/U	: Normalised velocity component in the x direction
GAC	: Generic Aircraft Carrier
TKE	: Turbulent Kinetic Energy
C_p	: Normalised pressure coefficient
P_i	: Local pressure
P_∞	: Reference atmospheric pressure
$C_{pi\ (Numerical)}$	: Normalised local pressure coefficient obtained by CFD
$C_{pi\ (exp)}$	: Normalised local pressure coefficient obtained by experiments
N	: Total number of pressure points
TI	: Turbulent Intensity
Fwd	: Forward
RMS	: Root mean square

Received : 31 October 2022, Revised : 11 April 2023
Accepted : 03 May 2023, Online published : 31 August 2023

1. INTRODUCTION

The aircraft carriers have been at the forefront since the pre-World War 1 era. Since then, the aircraft landings on a carrier at sea are a critical Naval Aviation operation and their importance and complexity have continued to increase over time. Due to the evolution of new geometries, greater payloads, technological advancements and endeavours of signature reduction, the complexity of the flight deck has increased. Extensive research has been conducted in the domain of aircraft carrier flight deck aerodynamics, which is considered to be the essence of flight operations onboard.

This research has covered a wide range of areas, from reducing pilot workload to visualising and modifying airflow patterns to improve performance. The landing onboard a flight deck of the aircraft carrier, spanning a few meters is the most challenging and complicated part of the entire aircraft operations. The turbulence generated by the various components of the flight deck, mostly by virtue of its design add on to the existing perturbations encountered by the pilot while attempting landing. These separated airflow regions varying in intensity propagate further downstream of the vessel, and are even encountered along the glidepath. The intensity of these fluctuations is at its maximum immediately aft of the carrier and is also prevalent within the last half a mile of the glideslope path, as reported by the pilots and, termed as the 'burble'[1]. The increased workload may lead the pilot and aircraft vulnerable to flight accidents as reported by Joshua[2], *et al.* and Wulfeck[3], *et al*.

The research in this domain dates back to the early 1950s and 1970s. The investigation of the flow dynamics

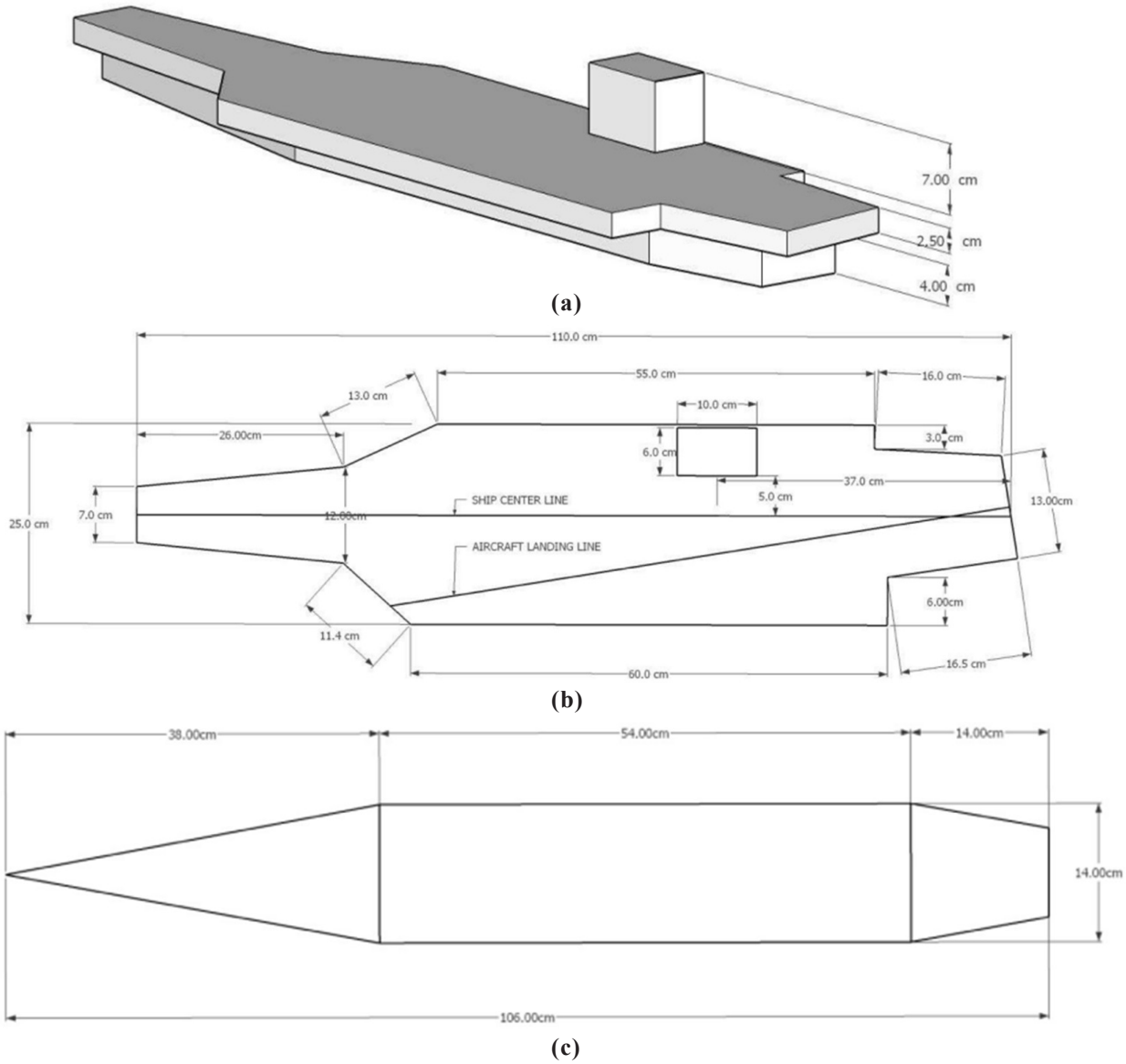

Figure 1. GAC detailed geometric dimensions: (a) GAC isometric view, (b) GAC flight deck top view and (c) Top view of hull dimensions.

in the vicinity of the flight deck has been undertaken experimentally[4-6,7-9] as well as computationally by various researchers[10-12] on the carriers. Also, the research has been undertaken for modification of flow by introduction of passive devices[13-15]. Cherry[1], *et al.* reported the burble phenomenon through various experiments on CVN-68, Nimitz class, and CVN-78, Ford-class carrier, and concluded that filleting of notches leads to a reduction in the intensity of vortex originating from the hull. The published literature[3-4,11-12] affirm that aircraft landing is riskier than launching and the flow features are certainly affected by the top deck layout and geometry.

The lack of data pertaining to aircraft carrier aerodynamics in open domain coupled with the absence of a standard benchmark research geometry, on similar lines of SFS and SFS 2 introduced by TTCP, initiated the introduction of a GAC geometry (Fig. 1) by Kumar[16-17], *et al.* at IIT Delhi. GAC has since been used to undertake numerical flow dynamics investigations by the introduction of ski jump[18]. Design drivers such as optimization of limited deck space availability necessitate the modification of the superstructure which led to origination of the twin island concept. The twin island concept has been spearheaded by the UK Navy and incorporated in the carriers HMS Queen Elizabeth and HMS Prince of Wales. Watson and Kelly[19-21], *et al.* published the airwakes for HMS Queen Elizabeth for flight simulation, however, the reported literature doesn't particularly signify the impact of the twin islands on pilot workload. Furthermore, there is a stark variation in the fundamental design of the HMS Queen Elizabeth and GAC in terms of inclination of the flight deck, with the GAC representing a 9° angled flight deck to a straight (0°) landing deck in Queen Elizabeth. Therefore, there is a requirement of exploring the flow over a twin island angled landing deck. View foregoing, GAC is equipped with a twin island design in the current study for investigating airflow dynamics over the subject geometry. The current study is a continuation of the studies undertaken on GAC to date and further enhances the research sphere of the aerodynamic flow over the carrier flight deck. This paper presents the twin island concept in

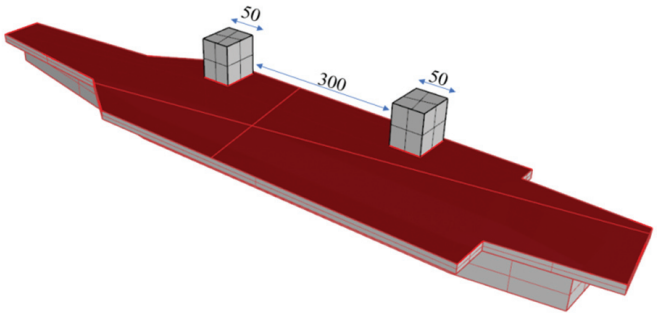

Figure 2. TGAC [All dimensions in mm].

GAC by splitting a single island on the flight deck into two distinct structures such that the overall area and volume remain unaltered i.e only the length is varied as seen in Fig. 2.

2. DETAILS OF GEOMETRY

The study encompasses the computational investigation of air wake aerodynamics on the TGAC (Twin Island Generic Aircraft Carrier) flight deck and parametric analysis for examination of the effect of longitudinal separation among the two island structures. The GAC geometry (1:300 scale model)[16] has been used as a yardstick for all the investigations in the present study including computations and validation as shown in Fig. 1. Details of the model are tabulated in Table 1. The GAC is placed in a wind tunnel cross-section of 0.75×0.45 m and 5.9 m long (Fig. 3) inclined at an angle of 9° so that the domain centreline aligns with the landing strip on the port of the island.

Taking cue from the findings of Shipman[12], *et al.* that the finer details of the geometric shape of the island have less influence on the far field flow characteristics, the study focussed on only splitting the island with no alteration to its original shape. The single island on GAC deck, has been bifurcated in two islands (each 50 % of original island length) and stationed longitudinally apart from each other (height and width remains same; the island is splitted only lengthwise). The aft island is at original GAC position and forward island is 3 times GAC island length forward of baseline position. The modified geometry has been referred to as TGAC for ease of understanding. The study aims to primarily identify and observe the airflow over the TGAC flight deck and secondarily investigate its impact on the pilot workload along the landing path (a 3-degree glide path as defined by ILS standards).

Table 1. Main particulars of GAC

Model scale		**1:300**
Model dimensions(L×B× Freeboard)(m)		1.1×0.25×0.065
Measure area of Flight Deck(m^2)		0.216
Island block dimensions(L×B×H)		0.1×.06×.07
Island position (m)	x from aft edge	0.41
	y from starboard edge	0.065
	from ship stbd edge to island stbd edge	0.0065

2.1 Computational Domain, Numerical Setup and Mathematical Formulations

Based on reported literature[19-24] the following boundary conditions were assigned for the subject problem: -

- Body and Bottom: Wall with no-slip.
- The inlet and outlet by the virtue of their function are assigned velocity inlet and pressure outlet respectively. The velocity at the inlet is taken as 15 m/s.
- Slip wall is given to the far field regions i.e., the top and sides of the domain.

Figure 3 is the pictorial representation of the computational domain alongwith boundary conditions.

The modelling was undertaken in Rhinoceros 3D and the simulations were carried out in STAR-CCM+ CFD tool. The finite volume method is utilised by the solver for discretization followed by solution of the governing equations and URANS (Unsteady Reynolds Averaged Navier Stokes equations). Eqns. 1 and 2 represent the governing equations of the present study derived from the continuity equation, momentum and energy Eqns.

$$\frac{\partial u_i}{\partial x_i} = 0 \tag{1}$$

$$\rho\left\{\frac{\partial u_i}{\partial t} + u_j \frac{\partial u_i}{\partial x_j}\right\} = -\frac{\partial P}{\partial x_i} + \frac{\partial}{\partial x_j}\left[\mu\left\{\frac{\partial u_i}{\partial x_j} + \frac{\partial u_j}{\partial x_i}\right\}\right] \tag{2}$$

The numerical setup details for the study are summarised in Table 2. The SIMPLE (Semi Implicit Method for pressure-linked equations) algorithm was used for pressure velocity coupling and the solution of governing equations. The flow solution was run for unsteady flow with a time step of 0.005 s. The convergence criteria was set as residuals < 10^{-6} [for continuity (u, v, w), momentum (x, y, z), tke, sdr (specific dissipation rate)] and was obtained in approximately 9000 iterations. Post convergence, the simulation was run for 0.8s

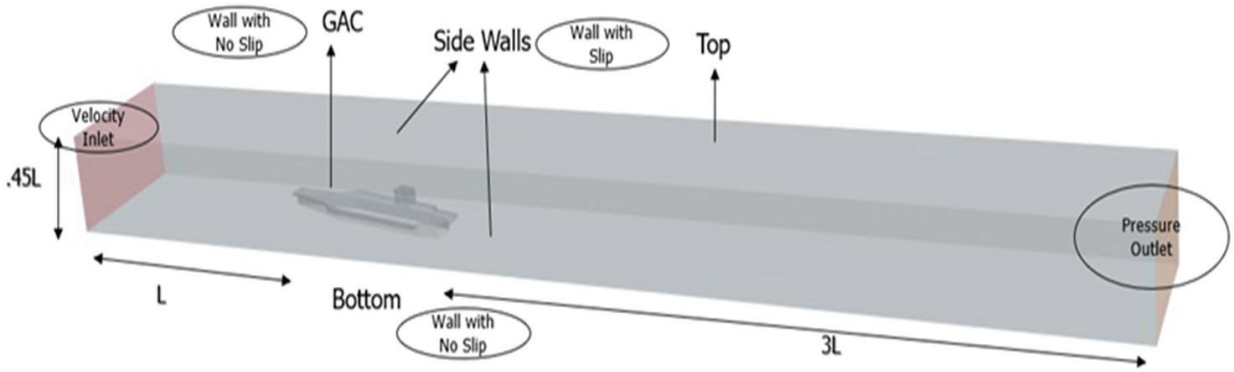

Figure 3. Computational domain.

Table 2. Numerical setup details

Solver	**3D segregated, implicit, unsteady**
Turbulence model	SST (Menter) k-w
Pressure discretisation	Standard
Wall treatment	All wall Y^+
Momentum discretisation	Second -order upwind
Pressure-velocity coupling	Coupled

to obtain time-averaged results which have been then used for analysis in the present study. The heading of the aircraft carrier is such that resultant relative wind velocity over the deck is along the landing line to aid the pilots while landing[4]. The Menter SST k-ω is selected for closure, principally due to its ability to capture the near as well as far fields with great precision as compared to other turbulence models and also as suggested by literature[2,16,19,25]. For the Menter SST k-ω model, the characteristic blending framework form is represented by Eqn. 3.

$$\Phi^{k\omega SST} = f\Phi^{k\omega} + (1-f)\Phi^{k\varepsilon},\ 0 \le f \le 1 \tag{3}$$

where, Φ is the modelled quantity and f is the blending factor.

2.2 Mesh Generation

A hybrid approach was adopted for grid generation and mesh generation was undertaken using trimmer mesh. Volumetric refinement is given to ensure full resolution of the flow close to the body, up to twice the length of the vessel. Also, grid is refined along the landing line (3° line from the landing point). Extra emphasis is provided to sharp corners and edges where anomalies may occur due to the convergence of successive grid growth areas. The grid alongwith the meshes and refinement regions is illustrated in Fig. 4.

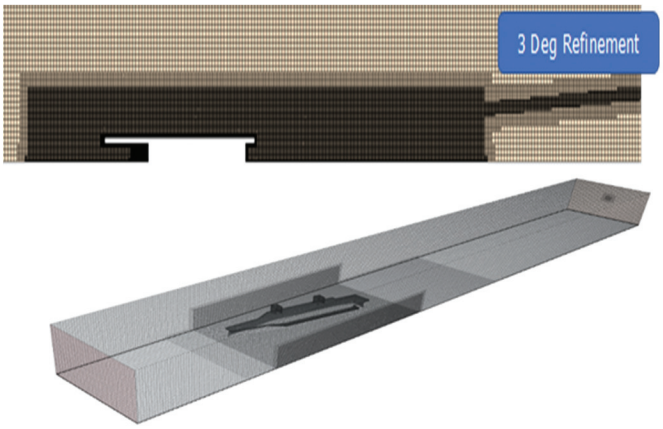

Figure 4. Computational mesh (side and top views).

Figure 5 shows the y^+ values obtained for the mesh generated. The y^+ values are less than one across the GAC body in accordance with the generalised wall y^+ values for k-ω SST turbulence model.

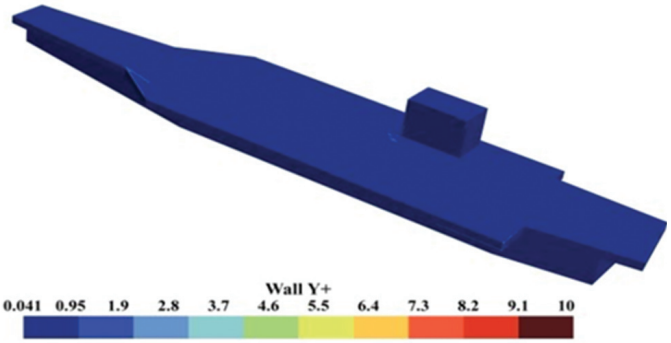

Figure 5. Wall Y^+ values.

3. EXPERIMENTAL VALIDATION OF CFD STUDY

Grid Convergence study was undertaken to ascertain the validation of the CFD model. The experimental data and results from the wind tunnel experiment conducted on GAC model at IIT Delhi[16] were taken for validation. The experimental pressure tapping's are replicated for the current study's validation part (Fig. 6). C_p, the pressure coefficient at any location, i, is defined by Eqn. 4.

$$C_p = \frac{P_i - P_\infty}{\frac{1}{2}\rho v^2} \tag{4}$$

The experimental and numerical pressure coefficients along various line are illustrated in Fig. 7(a)-(c). On comparison of the centre line results, we observe that the two curves follow similar trends and there are regions of reduced pressure in the vicinity of island structure attributable to bluff body behaviour. The comparable trend and general behavioural pattern of both the experimental and numerical pressure estimations along the port and starboard lines establishes the model's validation vis-a-vis the experimental setup.

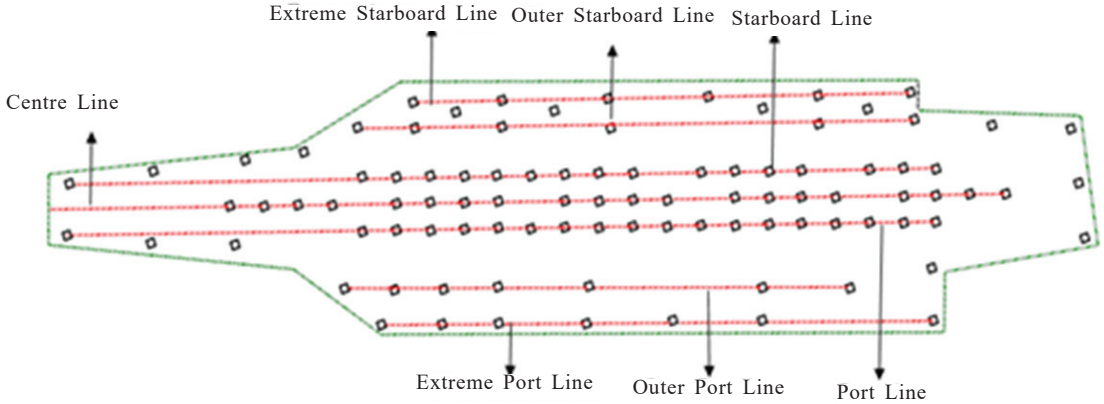

Figure 6. Pressure tappings replicated on GAC model.

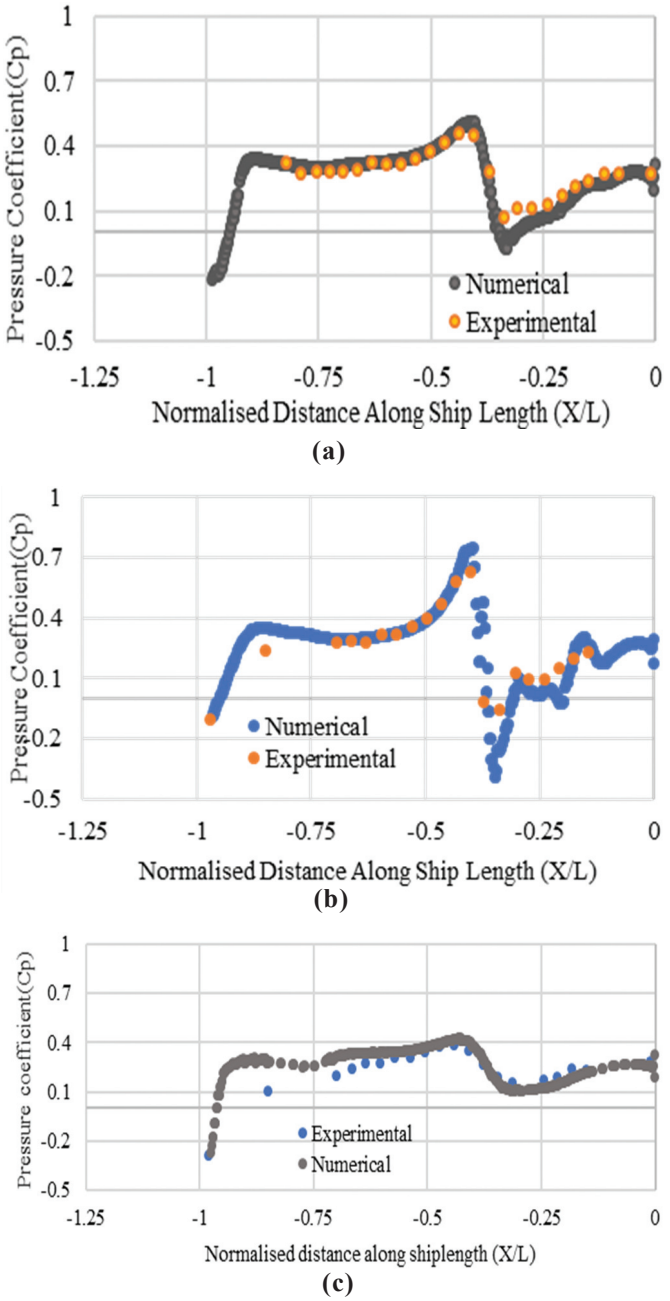

Figure 7. Experimental & numerical C_p plots, (a) Centre line C_p plots, (b) Starboard line C_p plots, (c) Port line C_p plots.

A root mean square relative error, as defined by Eqn. 5, is used for reporting the variation in the experimental and numerical results.

$$RMS\ Relative\ Error = \frac{1}{N}\sum_{i=1}^{N}\sqrt{\left(\frac{C_{Numerical} - C_{Experiment}}{C_{Experiment}}\right)^2} \quad (5)$$

where, $C_{Numerical}$ is the numerical pressure coefficient at any location, i, $C_{Experimental}$ is the experimental pressure coefficient, and N is the number of data points. When experimental and numerical dataset findings are compared, the highest differences found are ~6 %, regarded as a reasonably good compliance and acceptable within the conventional norms. This concludes the preliminary step towards validation of CFD results.

3.1 Grid Convergence

The grid sensitivity analysis and discretization error estimation was undertaken in accordance with the Richardson Extrapolation method introduced by Roache and further modified by Celik[25-26], *et al.* This method, unanimously accepted in engineering and CFD applications establishes the simulation's convergence with respect to grid size. Equation 6 is used for GCI determination.

$$GCI_{fine}^{21} = \frac{F_s \times e_a^{21}}{r_{21}^P - 1} \quad (6)$$

where, F_S is the factor of safety, e_a^{21} is the approximate relative error between grids 1 and 2 (Eqn. 7).

$$e_a^{21} = \left|\frac{\Phi_1 - \Phi_2}{\Phi_1}\right| \quad (7)$$

where, ϕ_i (i=1,2,3) represents the values of parameters (pressure and velocity) and r_{21} is the refinement depicted by Eqn. 8.

$$r_{21} = \frac{h_2}{h_1} \quad (8)$$

where, $h = \left[\frac{1}{N}\sum_{i=1}^{N}(\Delta V_i)\right]^{\frac{1}{3}}$, N = Number of cells or grids, ΔV_i = Volume of the grid at i^{th} location.

The grid sizes used for GCI analysis are tabulated in Table 3. The field quantities chosen as variables are pressure and normalized axial velocity along the glide path at the center aftmost point of the flight deck. The results of the grid convergence study are tabulated in Table 4. Based on the results, the streamwise axial velocity for Grid 2 and Grid 3

Table 3. Mesh details

Grid	Mesh size (Million cells)
A	8.98
B	6.32
C	4.38

Table 4. GCI

Description	Parameter – normalised axial velocity	Parameter – pressure
Number of cells (million)	8.98, 6.32, 4.38	8.98, 6.32, 4.38
Grid refinement ratio	1.414	1.414
Approximate relative error $\left(e_a^{21}\right)$	0.39 %	1.26 %
Approximate relative error $\left(e_a^{32}\right)$	0.75 %	2.99 %
Extrapolated related error $\left(e_{ext}^{21}\right)$	0.42 %	0.94 %
Extrapolated related error $\left(e_{ext}^{32}\right)$	0.81 %	2.19 %
Grid convergence index, GCI_{fine}^{21}	0.53 %	1.18 %

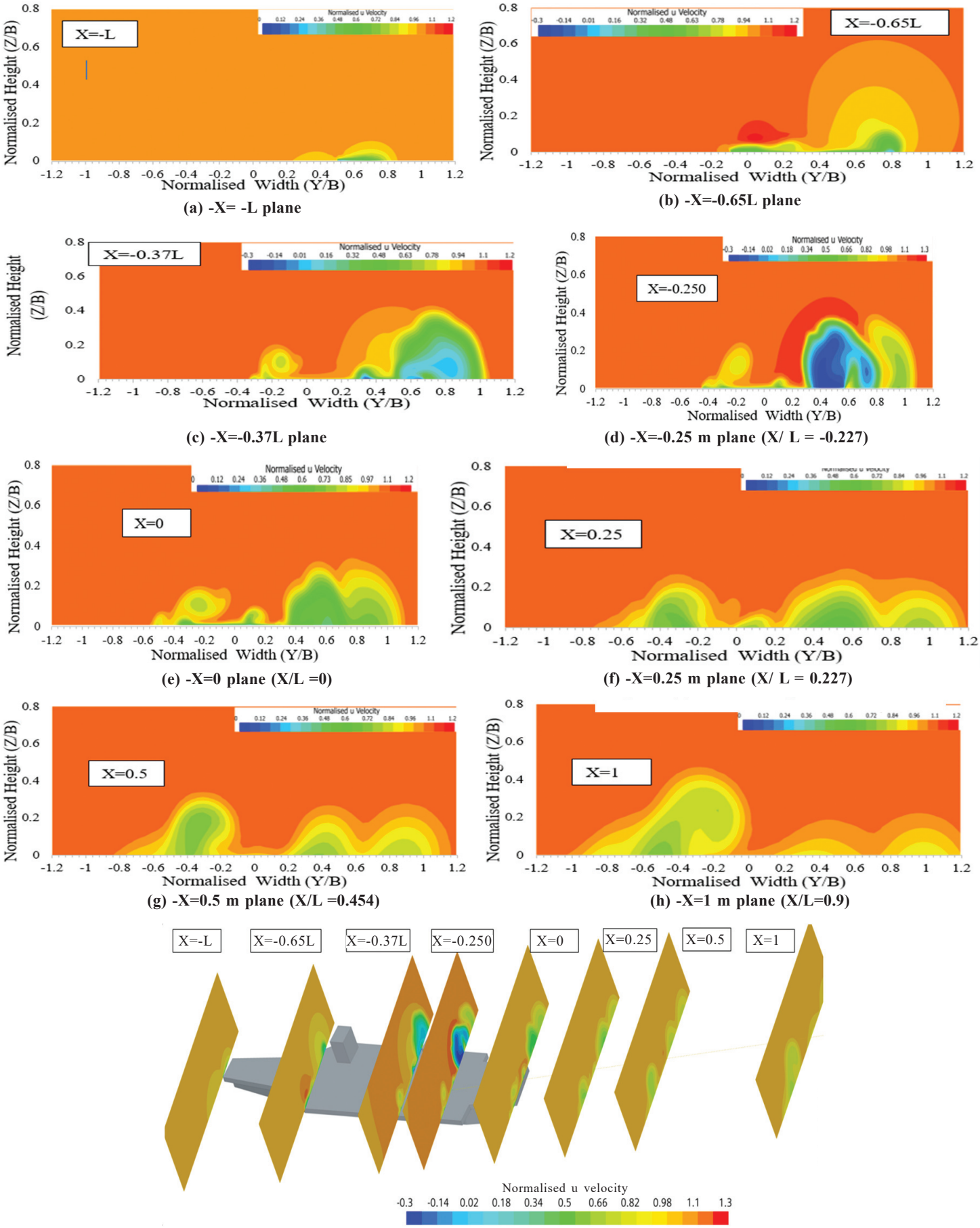

(a) -X= -L plane

(b) -X=-0.65L plane

(c) -X=-0.37L plane

(d) -X=-0.25 m plane (X/ L = -0.227)

(e) -X=0 plane (X/L =0)

(f) -X=0.25 m plane (X/ L = 0.227)

(g) -X=0.5 m plane (X/L =0.454)

(h) -X=1 m plane (X/L=0.9)

Figure 8. Velocity Plots across various X planes-TGAC.

have an error of only ~0.53%. This implies that Grid B, is most computationally efficient as there is not much change in the accuracy of results from B to C. Therefore, Grid B with mesh size of 6.32 million cells is used for undertaking further studies.

4. RESULTS AND DISCUSSIONS

The flow behaviour over the flight deck of the TGAC geometry (Fig. 2) is discussed in this section with pictorial and graphical representations. The flow parameters (velocity and turbulence) and the distances in each direction (x, y, z) are normalised with respect to ship's length, beam, and height to ensure standardisation of the obtained results. Normalised axial velocity and turbulence intensity are employed for understanding the flow behaviour on the flight deck as well as aft of the carrier.

4.1 Velocity Plots

The streamwise axial velocity assumes paramount importance for analysis of the aerodynamic behaviour on a flight deck. The aim of these plots is to capture and report the velocity variations as they occur and correlate with flow behaviour. Transverse planes (YZ planes) at various longitudinal distances from the domain centre are constructed [Fig. 8(a)-(h)] for flow analysis and quantification. These planes are perpendicular to the flow direction and parallel to transom of the GAC.

As the flow passes the forward edge of the GAC body, velocity systems induced by the separation at bow are formed as seen in the planes X=-L [Fig. 8(a)] and X=-0.65L [Fig. 8(b)]. The u/U~0.9 velocity contour bounded by a higher velocity region represented by u/U~1.02 indicates that the airflow has contacted bow and lifted off from the sharp bow edge. The contours at this plane represent two velocity deficient regions formation one on the port side with u/U~0.98 and one on the starboard side with u/U~0.8. The starboard side points to a larger velocity deficit owing to the stagnation zone at this region.

X=-0.65L plane indicates that the velocity deficit region on the starboard side has grown in area alongwith height. This plane is immediately aft of the forward shoulders, so the flow separation and generation of vortices from the port fwd shoulder is basis of the velocity deficit region (u/U~0.75) in this region and the higher velocity region(u/U~1.2) engulfing this deficit region confirms the same. The increment in velocity deficits on the starboard side is more than port side which can be related to the oblique placement of the GAC (9 deg to centre line) in the domain and the centre line plane intersecting the flight deck in a way that majority portion falls towards starboard side. Further moving downstream, at X=-0.37L [Fig. 8(c)], there is a marked increase in the velocity deficit regions on both the port and starboard sides. The flow here constitutes flow arising from interactions with bow, forward shoulders and forward island that has interacted with velocity deficit regions at these locations thus resulting in velocity deficits of order of u/U~0.2. Also, the velocity deficit region has shifted more towards the port side due to velocity stagnation region formed ahead of the backward island coercing the flow to take alternative route from the sides of the islands and influencing the flow patterns.

At X=-0.25 [Fig. 8(d)], the velocity deficit region has increased in height and width due to downstream movement of the flow. The two velocity deficits on the starboard side are due to two vortex systems created due to the flow interaction with the two islands. The reduction in height of the u/U~0.2 core on comparison with the previous plot indicates that the system from the forward island is getting weaker with the flow progression towards aft. Also, the port side region(u/U~0.9) has shifted further to port, an indicator of the resilient momentum possessed by the system on the port side that overcomes those created by the islands and while interacting with them still manages to maintain its strength despite losing a little momentum depicted by the velocity contours that hardly change on port side from X=-0.37L plane to X =-0.25 m plane. At the transom plane, the velocity deficits have shifted still further to the starboard side and the island created deficits i.e. the starboard deficit zones have drastically reduced from the previous view. The two island vortices also seem to be slowly influencing the port shoulder vortex at the transom.

Once the flow moves past the transom edge, the fwd shoulder and bow originated vortex motion also tugs in the vortices from the islands leading to reformation of velocity deficit regions as evident on the planes at X=0.25 m. Due to this phenomenon, the velocity deficit region in port side increases considerably in size and the starboard region diminishes. At the planes X=0.5 m and X=1 m, we see this region increasing further, an indication of the disturbance in the port side of the carrier downstream. This increasing turbulence is generally referred to as *burble* which directly impacts the landing trajectory and pilot workload as the increase in the velocity deficits leads to more thrust application from the pilot to maintain the aircraft's trajectory. From the plots as a whole, we can conclude that the velocity deficit region varies from u/U~0.2 to u/U~1.02 over one shiplength. The variations are more prominent over the deck region and diminish as the flow moves further aft and downstream of the flight deck. This is supplemented by the u/U~0.8-1.0 velocity contours on the X=1 plane.

4.2 Turbulence Intensity

In fluid dynamics, turbulence intensity(TI) is considered as a quantitative measure of turbulence occurring at a particular region. TI is plotted across Z=1 cm plane (Z/B =0.04) to observe the airflow on TGAC. Figure 9 shows that TI in the bow region varies from 15-19% and then it slowly comes down to 4–8% downstream. At the point when the flow interacts with the first island the value of turbulence rises to 21 % in the wake of the forward island, where it interacts with the aft island and turbulence again rises to 15-20 % in the wake of the island. The region between the two islands is highly turbulent with turbulence reaching to levels of 15–19 %. The turbulence which gradually is reducing along the downstream of the flow once again picks up at the transom attaining values of 10-12 % before gradually reducing to 4–7 %. This increment in the TI in the stern wake leads to instabilities in the velocities along the glideslope leading to potential increase in pilot workload.

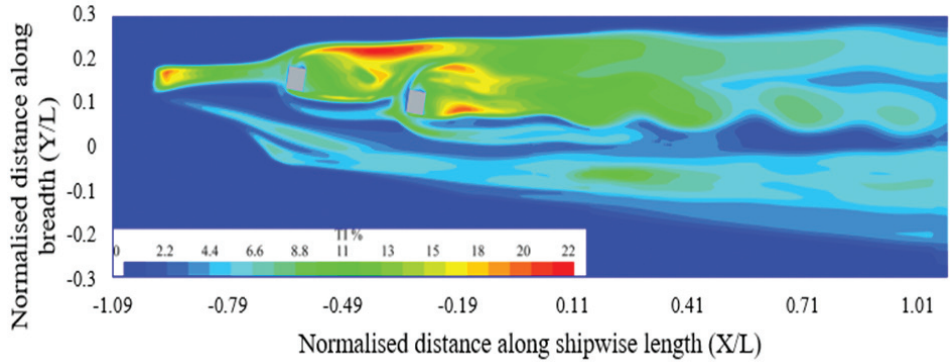

Figure 9. TI at z=10 mm (Z/B=0.04) -TGAC.

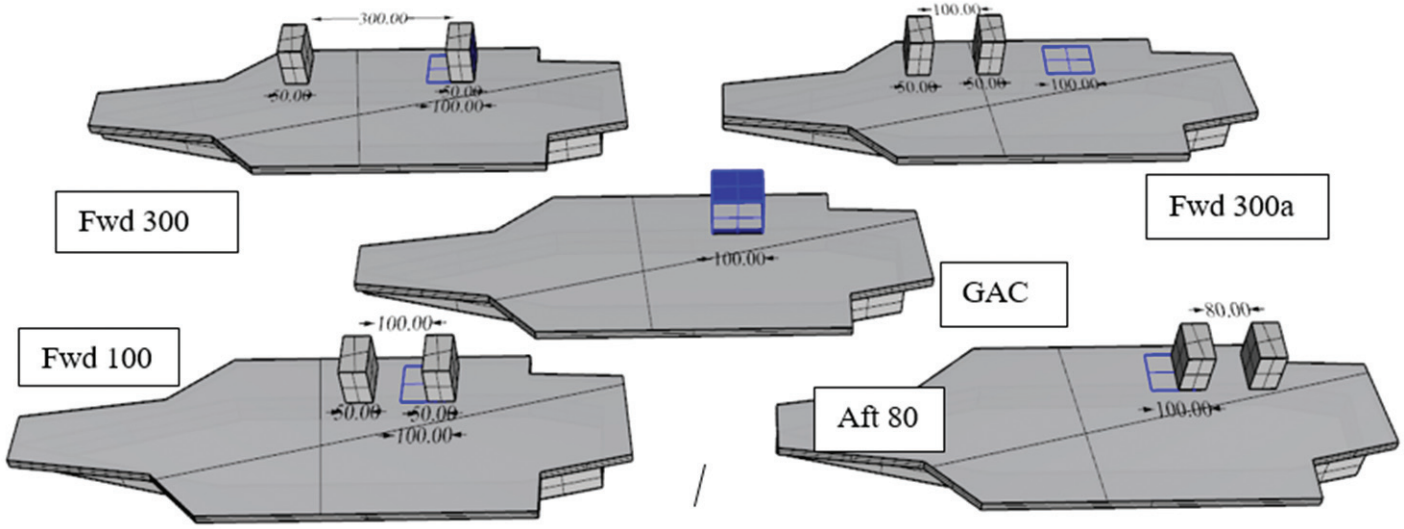

Figure 10. Variations of TGAC.

4.3 Parametric Studies

The positioning of the islands is the primary and foremost factor for finalisation of the carrier geometry which further dictates the number of aircrafts it can carry and operate, exhaust funnels positioning, maintenance area on the deck etc. Towards obtaining a clearer perspective in the longitudinal positioning of the islands with respect to aerodynamic performance and landing of aircraft and achieving the aforementioned, different variations are studied and investigated so as to obtain a general understanding of the concept. In all the variations, the basic geometry remains same, only the island's position is changed, that too longitudinally. The TGAC variations that are investigated are as follows: -

- TGAC Aft80 : It represents the configuration where the two islands on the flight deck are positioned such that, the aft island is spaced 80 % (wrt to original island length) aft of the forward island longitudinally. The fwd island is at original GAC island position and the aft island is stationed aft of this fwd island longitudinally; 0.8 times the GAC island length.
- TGAC Fwd100 : In this variant, the forward island is positioned 100 % ahead of the aft island lengthwise, the aft island being at original GAC island position.
- TGAC : When lengthwise, the forwards island is placed 300% fwd of the aft island (at baseline island position), the configuration is named as TGAC.
- TGAC 300a : In this variant, both the islands are moved forward longitudinally from the baseline position. The fwd island is positioned 300 % ahead of GAC position and the aft island is positioned such that the spacing between the two islands is one GAC island length. The resulting configuration is named as TGAC Fwd300a.

In all the configurations elaborated above, the % is in terms of original island length in GAC. This enables undertaking an all-inclusive comparative analysis and presentation of results in a simplified manner. Figure 10 depicts the pictorial representation of the TGAC variants.

A criterion has to be adopted for comparative study of the different geometrical variants of GAC. Velocity is the primary flow parameter required for any aerodynamic investigation, and its deficit or excess is assessed for flow quantification. Quantifying the turbulences the pilot would experience along the landing trajectory is also crucial and the most effective way to quantify this is in terms of turbulent kinetic energy. A lower TKE value is preferable since it denotes less fluctuations and disturbances along the glideslope, necessitating less pilot efforts to make adjustments and resulting in reduction in workload.

Additionally, it is envisaged to undertake analysis in terms of mathematical statistical tool, standard deviation. Standard deviation (Eqn. 9) is an accurate representation of the degree of data dispersion from the mean.

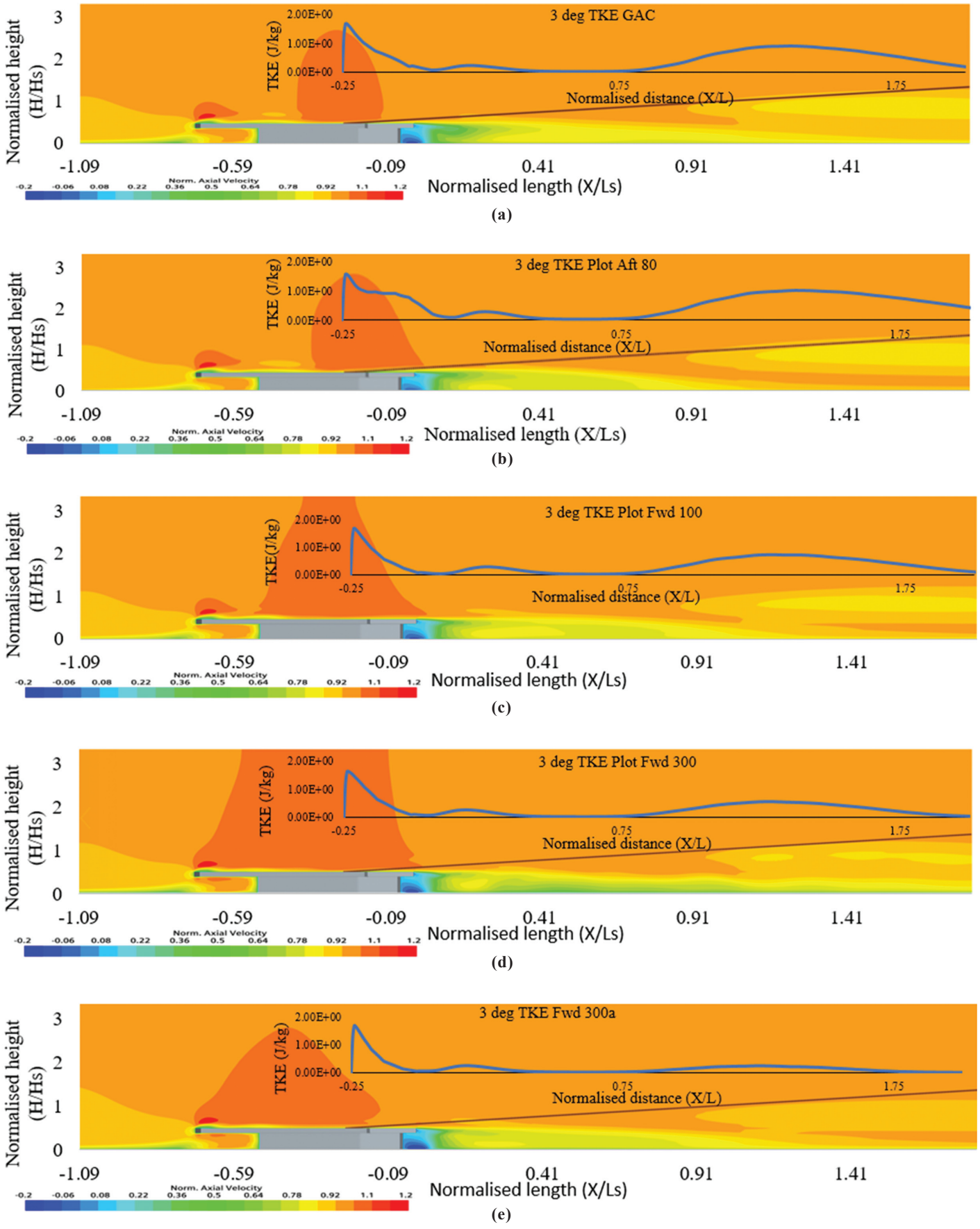

Figure 11. Combined TKE and normalised axial velocity plots along Y=0 plane for all variants, (a) GAC plots, (b) Aft 80 plots, (c) Fwd 100 plots, (d) Fwd 300 plots, and (e) Fwd 300a plots.

$$\sigma = \sqrt{\frac{\sum (u(x) - Mean)^2}{n}} \quad (9)$$

where, σ is standard deviation, $u(x)$ is normalised axial velocity, n is set size and mean is the freestream velocity.

Standard deviation has been used for illustration of the local flow velocity's departure from the ideal free stream velocity. Sequentially it communicates the magnitude of the approaching pilots' velocity deficit and translates to a brief loss of lift, which they must offset with increased thrust power, potentially adding to their workload. From the pilot perspective, a lower standard deviation is preferred.

A comparative representation of normalised axial velocity on a longitudinal plane, XZ plane passing through the landing line and origin, and TKE along glideslope is shown in Fig. 11. The plot exhibits the velocity changes as they occur downstream of the flight deck and vividly capture the stagnation, reversal and other flow variations across the flight deck and beyond. For all the variants, the normalised axial velocity gains in magnitude and intensity as it passes downstream about 0.75 L-0.8 L of the carrier wake where the effect seems to fade. However, the strength of the port vortex gains momentum with incoming strength from the island vortex due to which it grows in size in the region from 0.85 L–1.75 L. The occurrence of the above phenomenon is clearly evident as a region of u/U~0.85-0.97 in this length range. Alongwith this the increase in TKE plotted along the glideslope ascertains the burble presence. So, we can establish that the aircraft indeed encounters the disturbed flow or 'Burble' as the flow traverses through downstream.

Further, as the islands are spaced apart and moved forward, as in TGAC Fwd300a [Fig. 11(e)], an increase in normalised axial velocity and dip in TKE provide a confirmation of reduction in pilot workload. The configuration where the aft island is positioned aft i.e. Aft80 [Fig. 11(b)] exhibits maximum TKE making it aerodynamically unfavourable.

From the Fig. 12, it is evident that the majority of flow variations downstream along the landing line are occurring in two zones, the first one being from the landing point till 10% of shiplength and then from 1 L - 2 L. Both these areas are predominantly of the designer's apprehension as any changes in the velocity inflow or perturbations are likely to be supplemented by pilot actions like additional thrust/ lift augmentation snowballing the pilot workload towards maintaining the aircraft on the glidepath when he is very close to landing. The twin island variations in which the fwd island is positioned fwd of the original GAC island position, show a 5-7% increase in normalised axial velocity, which is deemed positive from the perspective of pilot effort, in the range of 1–1.6L. Overall, along the glideslope route from the landing site up to 1.8 times shiplength, a noticeable increase in the normalised u velocity is seen. This suggests that the twin island design helps to improve airflow over the landing path, hence lowering the number of course corrections the pilot must make. With an increase in the distance between the forward island and the backward island, which is in the baseline (GAC)location, the streamwise velocity is amplified proportionately. The increase of the u velocity is maximum when the backward island is also moved forward from the baseline GAC position (TGAC 300a) with the deficit in the streamwise velocity narrowing down to ~6–8 % in the 1.2–2L region.

The TKE variations (Fig. 13) along the landing line complements the findings of the velocity plot. When the front island is moved 300% ahead of the original GAC position for the TGAC variant, TKE decreases in magnitude by 35 % in the 1.2- 2L region, and this reduction is further attained up to 68 % when both islands are pushed forward of the baseline position (Fwd 300a). The similar trend of reduction in TKE is observed for all the fwd variations (except Aft80 variant), and TKE reduces by ~20 %, in comparison to GAC single island variant for the Fwd 100 variation also. There is a noticeable increase of 25-30 % in turbulence when the second island is moved 80 % aft of the baseline position and the first island is at the baseline position (Aft80).

The indices for flow comparison are tabulated in Table 5. The standard deviation of normalised axial velocity reduces as the forward island is positioned ahead of the original GAC position indicating that the alteration is having a positive effect on the pilot workload. The worst indices are obtained for the configuration when the backward island is shifted further aft

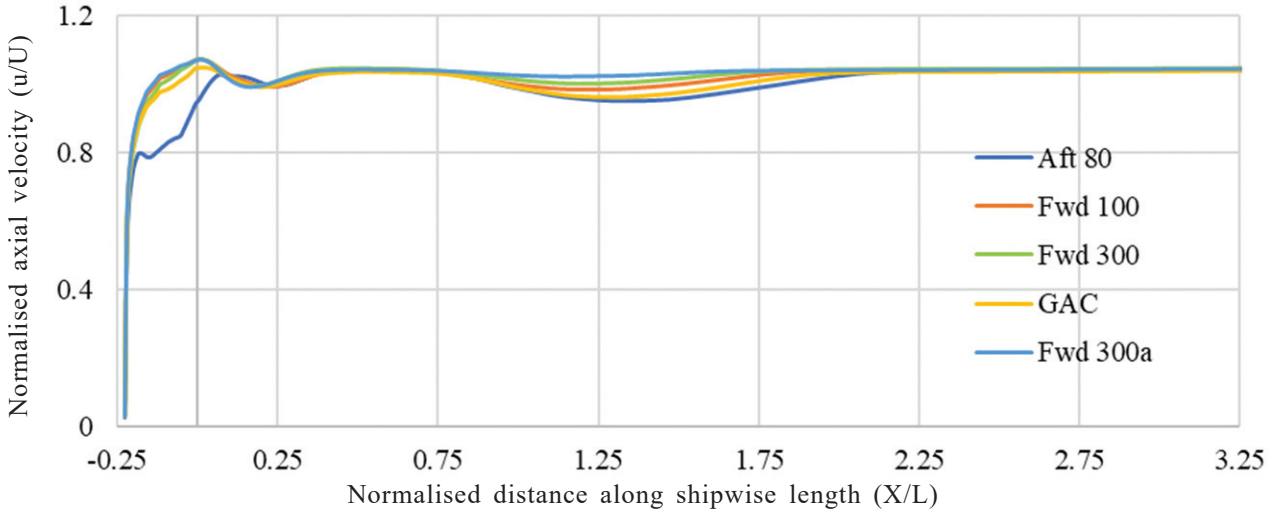

Figure 12. Normalised axial velocity plot-All variants.

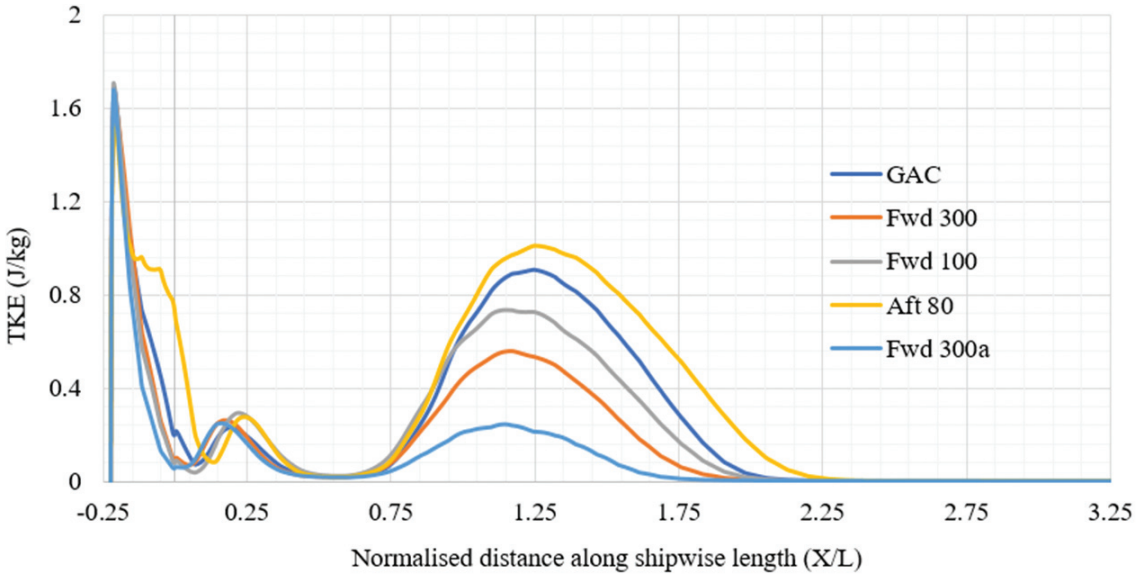

Figure 13. TKE along shipwise length.

Table 5. Flow indices for parametric investigation

Ser	GAC	TGAC	TGAC Aft 80	TGAC Fwd 100	TGAC Fwd 300a
Standard deviation in axial velocity (% of freestream velocity)	6.73	6.1	7.35	6.22	6.34
Net TKE(J/kg×m) along 3 deg	208.26	114.04	281.094	166.89	52.26

from its original position by 80 % making this configuration least favourable. From the Fig. 13, it can be concluded that the bulk of disturbance felt by the pilot improves substantially to 34 % in the TGAC variation and 20 % & 68 % for the Fwd 100 and Fwd 300a variations.

5. CONCLUSION

The study focussed on presenting alternatives to the conventionally single island approach on aircraft carrier's topdeck design. The subject study was undertaken by conducting URANS CFD simulations. The airflow as it passes the ship from the bow till transom and further aft of the carrier is analysed by the way of transverse planes cut across perpendicularly to the flow direction in the domain. Alongwith the normalised axial velocity, Turbulence Intensity along XY plane giving an insight on the areas where bulk of turbulence is encountered as the flow moves downstream of the carrier is also presented. Further the study includes the parametric analysis on different variants of the twin island configurations of GAC. The longitudinal separations of the two islands splitted from the single GAC island are then analysed with reference to GAC.

It is found from the parametric investigations and the flow visualisations that bluff body aerodynamics apply to the flight deck wind interactions and are more prominent around the sharp edges and sides that constitute the core of most disturbances. Once created, these disturbances are further felt and seen up to a significant distance downstream, even impeding and destructively interfering with the glide path of the incoming aircraft. As shown in the results and discussion section, dividing islands and translating forward of the baseline GAC island position has observable beneficial impacts on the burble along the glideslope. The aft translation (Aft80) of the divided island configuration is the least preferred variant and exhibits greater TKE and velocity deficits. The separation between the two islands, resembling backward-facing steps, plays a crucial role in the strength and stability of the recirculating flow. In particular, the Aft80 variation features a smaller spacing, resulting in a strong recirculating flow[27]. This, in turn, increases turbulence not only between the islands but also along the glideslope line and in the burble region, posing greater challenges and hazards during landing.

This option coupled with the reliability and survivability aspects that come along in the event of a major catastrophe to any of the engines, can be a viable option to look for in futuristic aircraft carriers. Additionally, there can be other variants (alteration of islands aspect ratios and inclusion of ski-jump) that are presently being studied at IIT Madras. The salient of the parametric study are elucidated as follows:

- It is beneficial to split the islands and translate forward, from aerodynamic point of view as compared to a single island.
- The aerodynamic advantage is maximum when both the islands are translated forward (TGAC 300a) and a substantial reduction in turbulence of the order of 68 % is obtained in this variant.

REFERENCES

1. Cherry, B. & Constantino, M. The burble effect-superstructure and flight deck effects on carrier air wake. United States Naval Academy, Annapolis, MD, 21412, 2010.

2. Handler, J. & Arkin, M.W. Naval accidents 1945-1988. Greenpeace/Institute for Policy Studies, Washington, D.C., Neptune paper no. 3, June 1989.
3. Brictson, C.A.; Pitrella, F.B. & Wulfeck, J.W. Analysis of aircraft carrier landing accidents (1965-1969). Dunlap and Associates, ONE, Washington, D.C., November 1969.
4. Lehman, A.F. An experimental study of the dynamic and steady flow disturbances encountered by aircraft during a carrier landing approach. *J. Aircraft*, 1966, **3**(3), 208–212.
   doi: 10.2514/3.43726.
5. Lamar, J.E.; Landman, D.; Swift, R.S. & Parikh, P.C. Subscale ship airwake studies using novel vortex flow devices with smoke, laser-vapor screen and particle image velocimetry. NASA Langley Research Center, Appendix X, 2005.
6. Wilkinson, D.T.; Zan, C.H.; Gilberts, J. & Funk, J. Modelling and simulation of ship air wakes for helicopter operations: A collaborative venture. *In* Proceedings of NATO, RTO Meeting on Fluid Dynamics Problems of Vehicles Operating Near or in the Air-Sea Interface, RTO-MP-15, Neuilly Sur- Seine, 1998.
7. Corporation, Dynasciences. An investigation of means of reducing aircraft carrier air turbulence to facilitate recovery of planes. Report No. DCR-205, Blue Bell, Pennsylvania, November 1966.
8. Ringleb, F.O. Three-dimensional smoke tunnel studies of wind over deck of aircraft carriers. *NAEL*, April 1963, NAEL-ENG-7019.
9. Mora, R.B; Montejano, B.M.; Rodriguez-Sevillano, A.A. & Leon-Calero, M. Wind flow investigation over an aircraft carrier deck by PIV. *Ocean Eng.*, 2019, **178**, 476–483.
   doi: 10.1016/j.oceaneng.2019.03.020
10. Polsky, S. & Bruner, C. A computational study of unsteady ship airwake. *In* RTO AVT Conference, 2001, 069, pp. 7–11.
    doi: 10.2514/6.2002-1022
11. Polsky, S. & Naylor, S. CVN airwake modeling and integration: Initial steps in the creation and implementation of a virtual burble for F-18 carrier landing simulations. *In* Collection of Technical Papers - AIAA Modeling and Simulation Technologies Conference 2005.
    doi: 10.2514/6.2005-6298
12. Shipman, J.; Arunajatesan, S.; Cavallo, P.; Sinha, N. & Polsky, S. Dynamic cfd simulation of aircraft recovery to an aircraft carrier. *In* 26th AIAA Applied Aerodynamics Conference, August 2008, pp. 1–11.
    doi: 10.2514/6.2008-6227
13. Nangia, R. & Lumsden, R. Novel vortex flow devices-columnar vortex generators studies for airwakes. *In* 34th AIAA Fluid Dynamics Conference, July 2004, pp. 1–18.
    doi: 10.2514/6.2004-2348
14. Mora, R.B.; Rodríguez, S.; Montejano, B. & Trigueros, N. Passive flow control over the ski-jump of aircraft carriers. *Ocean Eng.*, 2016, **114**, 134–141.
    doi: 10.1016/j.oceaneng.2016.01.019
15. Mora, R.B.; Rodríguez, S.; Calero, L. & Trigueros, N. Three-dimensional characterization of passive flow control devices over an aircraft carrier ski jump ramp. *Proceedings of Institute of Mechanical Engineers, Part G, J. Aerospace Eng.*, 2017.
    doi: 10.1177/0954410017716195
16. Kumar, K.V.; Nasiruddin, S; Shukla, S.; Singh, S.N; Sinha, S.S. & Rajagopalan, V. Pressure, and velocity measurements of air flow past a proposed generic aircraft carrier (GAC) geometry. *Proceedings of the Institution of Mechanical Engineers, Part M: J. Eng. Maritime Environ*. 2021.
    doi: 10.1177/14750902211048958
17. Kumar, K.V., Mathew, M.P.; Singh, S.; Sawan, S.N. & Rajagopalan, V. Experimental investigation of flow over the flight deck of a generic aircraft carrier. *In* Warship 2018- Procurement of Future Surface Vessels, 2018.
18. Thakur, R. & Kumar, K.V. Investigation of the effect of ski jump on the flow dynamics around generic aircraft carrier, *Defence Sci. J.*, March 2021, **71**, 296-303.
    doi: 10.14429/dsj.71.15648
19. Kelly, M.F; White M.D.; Owen I. & Hodge, S.J. The Queen Elizabeth class aircraft carriers: airwake modelling and validation for astovl flight simulation. *In* American Society of Naval Engineers, Launch and Recovery Symposium 2016, MITAGS, Linthicum Height. Maryland, USA, December 2016.
20. Kelly, M.F.; Watson N.A.; Owen I.; White M.D. & Hodge, S.J. The role of modelling and simulation in the preparations for flight trials aboard the Queen Elizabeth class aircraft carriers. *In* 14th International Naval Engineering Conference 2018, Glasgow, UK, October 2018.
    doi: 10.24868/issn.2515-818x.2018.037
21. Watson, N.A.; Kelly, M.F.; Owen, I.; Hodge, S.J. & White, M.D. Computational and experimental modelling study of the unsteady airflow over the aircraft carrier HMS Queen Elizabeth. *Ocean Eng.*, 2019, **172**, 562–574.
    doi: 10.1016/j.oceaneng.2018.12.024
22. Forrest, J.; Owen, I. & Padfield, G.D. Ship-helicopter operating limits prediction using piloted flight simulation and time-accurate airwakes. *J. Aircraft,* 2012, **49**(31), 1020–1031.
    doi: 10.2514/1.C031525
23. Shukla, S.; Sinha, S.; Saroha, S. & Singh, S.N. Experimental and computational investigation of airwake aerodynamics of the generic aircraft carrier with ski-jump. *Ocean Eng.*, 2022, **249**.
    doi: 10.1016/j.oceaneng.2022.110902
24. Kelly, M.F.; White, M. & Owen, I. Using airwake simulation to inform flight trials for the Queen Elizabeth Class Carrier. *In* 13th International Naval Engineering Conference, Bristol, UK, 2016. https://livrepository.liverpool.ac.uk/id/eprint/2053661
25. Celik, I.B. Procedure for estimation and reporting of discretization error in CFD applications. *ASME. J. Fluid Eng.*, 2008, **130** (7).
    doi: 10.1115/ 1.2960953.
26. Crippa, S. Improvement of unstructured computational

fluid dynamics simulations through novel mesh generation methodologies. *J. Aircraft*, 2011, **48**, 1036–1044. doi: 10.2514/1.c031219

27. Mcqueen, T.; Burton, D.; Sheridan, J. & Thompson, M.C. The double backward-facing step: interaction of multiple separated flow regions, *J. Fluid Mechanics*, 2022, **936**. doi: 10.1017/jfm.2022.9

CONTRIBUTORS

Lt Cdr Ankit Nehra is a graduate of Naval Architecture from CUSAT and PG Diploma in Naval Construction from IIT Delhi. His fields of interest include: Warship design, Computational fluid dynamics, Aircraft carrier studies, and Ship aerodynamics.

In the current study, he has conceptualised the study, modelled the geometry and performed computational simulations for the subject problem solution. Also, the interpretation of the results and analytical analysis has been done by him.

Cdr (Dr) R. Vijayakumar obtained his PhD from IIT Delhi. He is presently working as Associate Professor at Dept of Ocean Engineering at IIT, Madras. His fields of interest include: Warship design, Ship hydrodynamics, Ship dynamics and Computational Fluid Dynamics (CFD).

In the current study, he has provided guidance on the analysis and interpretation of the data, and manuscript preparation.